Fire Safety Journal 157 (2025) 104489

Contents lists available at ScienceDirect

Fire Safety Journal

journal homepage: www.elsevier.com/locate/firesaf

Insight into laboratory-scale junction-fire dynamics using 3-D physics-based numerical simulations

Ahmad Hassan [a,*], Gilbert Accary [b], Jason Sharples [c], Khalid Moinuddin [a]

[a] Institute for Sustainable Industries and Liveable Cities, Victoria University, Melbourne, Australia
[b] School of Engineering, Lebanese American University, Byblos, Lebanon
[c] University of New South Wales, UNSW Canberra, Australia

ARTICLE INFO

Keywords:
Extreme fire
Merging forest fires
Bushfire modelling
Fire-driven wind
Large-eddy simulation

ABSTRACT

Junction fires exhibit complex behaviour and are characterised by unique physical processes, which have attracted considerable interest in the wildfire community. This paper provides an in-depth analysis of junction-fire dynamics, leveraging numerical simulations to understand the mechanisms responsible for fire-spread deceleration observed experimentally and to provide insights about the characteristics of fire-induced wind. Using the FIRESTAR3D model, a fully physical, CFD, wildfire simulator, junction fire simulations were conducted at laboratory scale under various junction angles, terrain slopes, and prescribed wind speeds. An analysis of the interaction between the flow field and the flames' structure was carried out. Results show that the deceleration phase of junction fire propagation, observed experimentally at small junction angles on a horizontal terrain with no imposed wind, is due to a change in the flame direction preceding the fire-spread deceleration, resulting in a decrease in the interaction between the arms of the junction fire. The study also provides a better understanding of the action of fire-induced wind and competition with the prevailing wind in shaping the junction fire flames. This study offers new insights into the complex dynamics of junction fires, and the analysis of induced wind supports the development of comprehensive scaling laws for their behaviour.

1. Introduction

Junction fires, where two fire fronts intersect at an oblique angle, have attracted considerable attention in recent years due to their enhanced rate of spread and associated intensity. Notable incidents involving a junction fire, compounded by the influence of large-scale dynamic processes, occurred in the devastating junction fire near Pedrógão Grande, Portugal, on June 17, 2017 [1], and the merging fires that occurred near Canberra, Australia, on January 18, 2003 [2,3]. These fires, characterised by their extreme behaviour and rapid spread, pose significant risks to firefighter and community safety and to the environment and wildlife. For these reasons, junction fires have drawn considerable attention in the wildland fire community, and studies have identified various factors contributing to the extreme behaviour of junction fires, such as enhanced convective processes and intensified fire coupling mechanisms. Junction fires are of interest in that they exhibit both conventional fire behaviours influenced by external conditions (e.g., wind, slope, and fuel characteristics) and additional intensifying effects caused by the interaction of the merging fire fronts. Viegas et al. [2] conducted seminal laboratory-scale junction fire experiments, explaining the rapid junction fire spread, driven by a high concentration of energy near the junction point, which differs from traditional convective energy transport along a fire line. Building on this research, Viegas et al. [4] extended the analysis by investigating the effects of fuel bed compositions and terrain slope on junction fire behaviour. This work revealed that junction fires exhibit varying rate of spread (ROS) depending on the slope, with steeper slopes leading to accelerated fire spread. Notably, Viegas et al. [4] showed that fuel composition does not have a significant impact on the overall fire behaviour. Sharples et al. [5] studied the merging of oblique fire fronts and proposed a model that links the curvature of the fire line to energy accumulation, contributing to an enhanced ROS at the junction point. Thomas et al. [6] expanded Sharples et al.'s study by considering the effects of pyroconvective coupling (convection induced by the presence of the fire) between the merging fire lines, showing that this coupling could lead to a substantial increase in the ROS. Hilton et al. [7] introduced a pyrogenic potential model to simulate near-ground airflow effects in wildfires, based on fire line intensity. It effectively predicts fire perimeter behaviour, including

* Corresponding author.
E-mail address: ahmad.hassan6@live.vu.edu.au (A. Hassan).

https://doi.org/10.1016/j.firesaf.2025.104489
Received 3 January 2025; Received in revised form 28 July 2025; Accepted 30 July 2025
Available online 31 July 2025

parabolic fire shapes and junction fire closure, with computational efficiency and potential for operational use. Sullivan et al. [8] further examined the influence of the junction angle on fire behaviour in dry eucalyptus litter under calm and windy conditions. The study showed that while calm conditions led to weak fire interactions, wind significantly enhanced the fire spread within the junction. The very small scale (1 and 1.5 m arms) of their experiments may have led to discrepancies under calm conditions with previous studies. Recent technological advancements, such as the use of UAVs for data collection [9], allowed researchers to better capture fire behaviour and the ROS in real-time at large scale. Filkov et al. [10] conducted preliminary field experiments using UAVs, which revealed significant variations in the ROS across different junction fires and parallel front fires. These findings raised important questions regarding the impact of fire size, fuel structure, and wind speed on fire propagation, emphasising the need for standardised experimental conditions and improved data collection methods. Holyland et al. [11] extended the analysis of junction fires using thermal footage from drones and on-ground measurements to assess how merging fire fronts affect fire behaviour. Interestingly, wind speed was found to have little influence on fire behaviour, suggesting that factors such as junction geometry are more critical in junction fires. Raposo et al. [12] conducted laboratory-scale junction fire in a shrub fuel bed and pointed out that the junction point speed increases very rapidly owing to strong convective effects created by the fire that are similar to those of an eruptive fire. Using fully-physical modelling, junction fires were successfully replicated, showing good agreement at both qualitative and quantitative levels [13]. Subsequent studies [14,15] extended these initial simulations through a parametric study, revealing important characteristics of junction fires for different junction angles, terrain slope and prescribed-wind speed. Both experimental and numerical studies [12,14,15] have shown that the spread of junction fires is mainly governed by the junction angle and that the dominant heat transfer mode mainly depends on terrain slope and wind speed. Fires with small junction angles spread rapidly and exhibit abrupt increases in ROS, while fires with larger junction angles spread more slowly. Even for wide junction angles, the interaction between the junction fire arms accelerates the propagation of the fire, leading to a higher ROS than would be expected from two independent fire fronts.

Despite advancements in this field, including small-scale and large-scale experimental studies and modelling efforts, a comprehensive understanding of the mechanisms driving these behaviours remains elusive. For instance, one intriguing behaviour is the fire-spread deceleration phase observed under certain conditions at the end of junction fire propagation [2]. Indeed, when two fire fronts merge together, the junction point accelerates to reach a maximum ROS. Then, depending on the fire parameters, fire acceleration may continue until fuel is depleted, or it may undergo a deceleration phase, during which the angle between the junction fire arms progressively increases while the ROS progressively decreases. This decelerative behaviour does not occur under imposed wind conditions or on inclined terrain (at least when wind or slope directions are aligned with the junction axis), where junction fires exhibit more dynamic behaviour. Raposo et al. [12] explored the deceleration phase in junction fire spread, proposing that flow properties and convective processes play a central role in controlling fire behaviour. Raposo et al. also suggested that radiation dominates during the deceleration phase and that the fuel type has minimal impact on the fire dynamics. This deceleration phenomenon was also observed by numerical simulation [14] and results showed that the fire spread deceleration occurs for junction angle less than 45° and this goes along with an increase in the angle between the junction fire arms, confirming the experimental observation [12]. However, the underlying physics of such behaviour has never been addressed. Another poorly understood aspect, is the role played by fire-generated flow, commonly known as the induced wind, which, under weak wind and no slope conditions, plays a crucial role in shaping the flames of a junction fire. Examining the action of the induced wind is hence important for better understanding the behaviour of junction fires and, ultimately, for developing scaling laws for junction fire behaviour, in a similar way to what has been developed in the literature for a single fire front [16]. This is essential for improving predictive fire models [17] and enhancing the accuracy of fire behaviour forecasts and firefighting.

By numerically reproducing laboratory-scale experiments of junction fire [12] using the fully physical model FIRESTAR3D [18] and by examining the characteristics of flames and flow fields surrounding the flaming zone, this study seeks to address the knowledge gap in junction fire behaviour. The primary focus is to provide a deeper understanding of the unique behaviours in junction fires, particularly the reasons behind the transition between the acceleration and the deceleration phases of fire spread, in addition to providing insights about the fire-flow interaction under various conditions of junction angle, terrain slope and prescribed-wind speed. By leveraging physics-based simulations, this study advances the understanding of junction-fire dynamics and offers insights in complex dynamic phenomenon [19] and their sensitivity to certain environmental or wind factors.

2. Modelling and numerical method

FIRESTAR3D is a fully physical, Computational Fluid Dynamics (CFD) model, based on a multiphase formulation [18,20]. The model predicts the behaviour of the coupled system consisting of a turbulent-reactive gaseous flow (fluid phase) interacting with a vegetative fuel (solid phase) represented as a porous medium. A summary of FIRESTAR3D model is provided in Appendix A.

Fig. 1 shows the problem configuration, and the computational domain considered in this study. A V-shaped fuel-bed is considered on inclined terrain (making an angle α with the horizontal plane) with 5 m-long arms. Terrain inclination was accounted for by considering two gravity components: $g_z = -g\,cos\,\alpha$ and $g_x = -g\,sin\,\alpha$. As in the experiments of Raposo et al. [12], a 15 cm-thick homogeneous layer of shrub is used with the following properties: fuel volume fraction $\alpha_S = 0.00784$, surface-to-volume ratio $\sigma_S = 6900\ m^{-1}$, dry material density $\rho_S = 500$ kg m^{-3}, dry fuel specific heat $C_S = 1380$ J kg^{-1} K^{-1}, and moisture content $M = 20$ %. The particles were assumed to be thermally thin and to behave as a black body. Furthermore, the particles were assumed to have cylindrical shape with a drag coefficient $C_D = 0.42$ [13]. Open boundary conditions were applied to all sides of the computational domain except the bottom one, where a solid-wall condition was imposed.

Before ignition, a one-seventh power-law velocity profile given by Eq. (1) was applied at the inlet (with $z_0 = 1$ m) resulting in the desired 1-m open-wind velocity (U_0), while Neumann conditions (i.e., zero normal-gradient) were applied at the open boundaries. Before ignition, simulations were run long enough to reach statistically steady flow conditions.

$$U(z) = U_0\left(\frac{z}{z_0}\right)^{1/7} \tag{1}$$

Fuel is ignited by injecting CO at 1600 K from the bottom of the computation domain for 5 s along the firearms (burner width was 10 cm), according to the procedure described in Frangieh et al. [16]. The average injection speed was 10 cm/s at the beginning of the ignition phase, then it was decreased linearly with the burned mass of dry material in order to avoid destabilising the fire-front by suddenly ceasing the injection. It should be noted that, based on CO combustion heat (10.112 MJ/kg) and the burner parameters, the maximum burner power was about 2.15 kW per meter of junction arm length and was negligible compared to the fire intensity. After ignition, the inlet boundary condition was modified: a Neumann condition was applied at the domain inlet (i.e., zero normal-gradient for all variables) and a pressure gradient was applied in the x-direction to maintain wind velocity constant far from the fire front, 1 m above the ground (at point A in Fig. 1-b), while

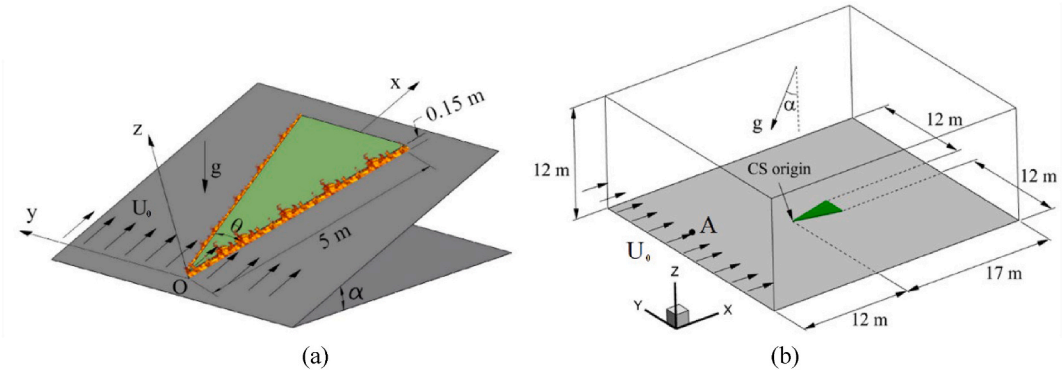

Fig. 1. (a) Junction geometry and problem parameters (junction angle θ, slope angle α and wind speed U_0). (b) Computational domain used to simulate a junction fire, CS: coordinate system.

allowing the fire front to withdraw fresh air from the domain inlet. This inlet condition allows for induced wind to occur at the domain inlet while maintaining the prevailing wind speed far from flaming zone [20].

A uniform mesh with cells size (Δx, Δy, Δz) = (2.5 cm, 2.5 cm, 1.25 cm) was used for the solid phase, while a non-uniform mesh of 160 × 160 × 160 cells was used for the fluid phase. Within the vegetation zone, the fluid-phase grid was uniform with (Δx, Δy, Δz) = (5 cm, 5 cm, 2.5 cm) and then it was progressively coarsened toward the open boundaries. It should be noted that for both the fluid and the solid phases, the grid cells-size was below radiation-extinction length-scale given by $4/\alpha_S\sigma_S$ [21] and equal to about 7.4 cm in this case. Details of the mesh structure are given in Appendix B.

In this study, full physical modelling of junction fires was performed for θ = 15, 30 and 60°, for α = 0 (horizontal terrain), 20° and 30°, and for U_0 = 0 (no prescribed external wind), 1 and 3 m/s. The simulations analysed in the present study to understand the mechanisms responsible for fire-spread deceleration were part of broader parametric studies [14,15] carried out to describe the effects of the junction angle, slope and wind speed on junction fire behaviour (mainly the ROS) and the dominant heat transfer mode.

It should be noted that FIRESTAR3D model has extensively been validated in various vegetation fire configurations [13,16,18,20,22]. In particular, for the configuration of a junction fire, the model has been validated [13] using data collected from laboratory experiments conducted by Raposo et al. [12]. In addition, a mesh-sensitivity analysis was conducted and is included in Appendix B. Finally, a summary of previously reported results [14,15], describing the effects of terrain slope, junction angle, and wind speed on junction fire global behaviour, is provided in Appendix C.

3. Results and discussion

For the sake of clarity and in order to avoid combined effects of problem parameters on fire behaviour, the results section is subdivided into two parts: 1 – Junction fire on horizontal terrain with no applied external wind, for which the deceleration phase of junction fire spread is observed experimentally, 2 – Slope and wind effects considered independently. For both sub-sections, a discussion of the ROS is provided,

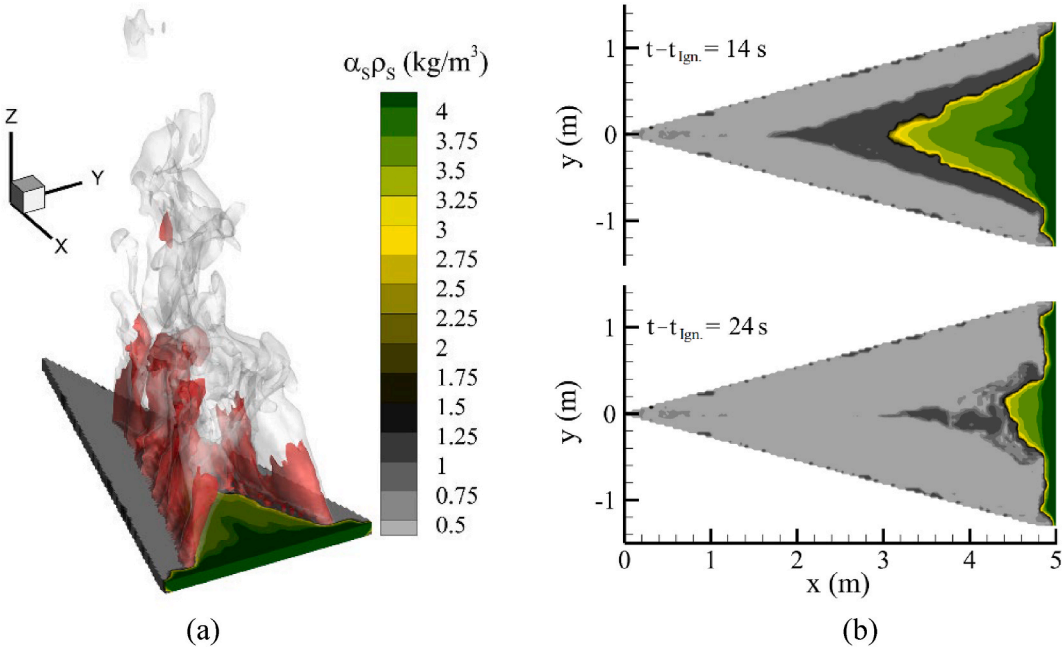

Fig. 2. (a) Junction fire for a junction angle θ = 30°, obtained numerically 14 s after ignition on a horizontal terrain with no applied external wind. Flames are visualised by the temperature iso-value surface T = 1000 K, smoke is visualised using CO_2 mass-fraction iso-value of 0.05 (with 75 % transparency), vegetation decomposition is visualised by fuel bulk-density. (b) Distribution of fuel bulk-density at the vegetation top-surface obtained for a junction angle θ = 30° obtained 14 s and 24 s after ignition on a horizontal terrain with no applied external wind.

followed by a comprehensive description of flame structure, flow dynamics, and mode of fire spread.

3.1. Junction fire on a horizontal terrain with no applied external wind

Fig. 2(a) shows a 3D view of the numerical solution obtained 14 s after ignition for a junction angle $\theta = 30°$, where vegetation decomposition is visualised by the fuel bulk-density $\alpha_S\rho_S$. The pyrolysis-front position at the fuel-bed top-surface can be easily located in Fig. 2(b) from the distribution of fuel bulk-density; it corresponds to the transition from black to yellow colour. One of the main parameters of junction fires is the ROS of the junction point obtained by tracking the pyrolysis-front position, which corresponds to the most advanced point along the junction axis with a dry-material mass-fraction equal to 0.

The time evolution of the junction point position is shown in Fig. 3 for three values of the junction angle in the case of horizontal terrain with no applied external wind. The ROS of the junction point corresponds to the slope of these curves. As previously shown both experimentally [2,12] and numerically [14], the junction point ROS increases as the junction angle θ decreases. For a junction angle of 15 and 30°, Fig. 3 shows the existence of a deceleration phase (shown by vertical segments) before the junction point reaches the end of the fuel bed, which does not occur for $\theta = 60°$ (where a quasi-constant ROS is obtained throughout the simulation); this behaviour was also reported experimentally [12]. It should be noted here that for all three junction angles, the junction point had reached the end of the fuel bed, but the fuel-bed length was not the same for all three cases. Indeed, since 5 m-long junction fire arms are considered for all θ values, the fuel-bed length is equal to 5m × cos(θ/2). For $\theta = 15$ and 30°, a 5 m-long fuel bed was considered since cos(θ/2) is close to 1, while a 4.3 m-long fuel bed was considered for $\theta = 60°$. This explains the final junction point position as the fire reaches the end of the fuel bed.

To better understand the reasons behind this deceleration phase only observed in the case of small junction angles, no slope and no applied external wind, a detailed analysis of the interaction between the flames and the surrounding flow field was carried out at different times of propagation. As can be seen from the temperature field shown in Fig. 4 for $\theta = 30°$, a change in the flames' inclination occurs between $t - t_{Ign.} =$ 14 s and $t - t_{Ign.} = 24$ s. At $t - t_{Ign.} = 14$ s, the flames are tilted forward towards the unburnt vegetation as shown by the horizontal cuts of the temperature field at $z = 0.3$ m and 0.6 m, where the green line corresponds to the borders of flame at the vegetation top-surface. At $t - t_{Ign.} =$ 24 s, the flames are vertical since the temperature patterns at $z = 0.3$ m and 0.6 m are within the green outline. This represents a vertical flame structure. Another remarkable observation is the change in the junction angle obtained in this case during fire propagation. At $t - t_{Ign.} = 14$ s, the angle between the junction fire arms remains at about 30°, while it noticeably increases at $t - t_{Ign.} = 24$ s, particularly at the unburnt-fuel side. Similar but faster and more pronounced behaviour was observed for $\theta = 15°$ owing to the very close arms in this case. For $\theta = 60°$, no change in the flames' inclination and in the angle between the junction fire arms was observed. Indeed, as shown by Fig. 5, the flames remain practically vertical throughout the entire simulation time with no change in the angle between the junction fire arms. This increase in the angle between the junction fire arms that occurs at small junction angles is the reason behind the deceleration in the junction point motion, since the ROS of the junction point decreases when the junction angle increases as previously reported [2,12,14] and shown in Fig. 3.

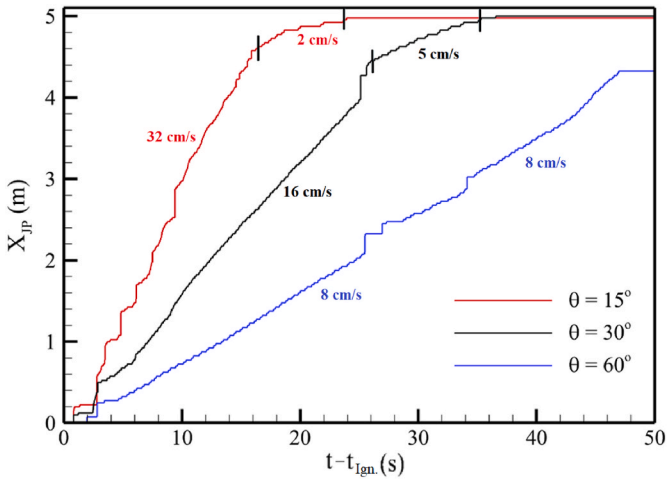

Fig. 3. Time evolution of the junction point position for different junction angles in the case of a horizontal terrain with no applied external wind. Average ROS values are indicated at different phases of fire propagation. The vertical segments show the deceleration stages.

To determine the origin of this change in the angle between the junction fire arms, the flow around the fire is depicted in Figs. 6 and 10 for $\theta = 30°$ and 60°, respectively, in the case of a horizontal terrain with no applied external wind. The velocity-field vectors are represented indicating the direction and magnitude of the flow velocity (1 m/s magnitude vector is shown for reference). In both cases, the flow is drawn from all directions towards the V-shaped flaming zone. The flow between the fire-arms is in the opposite direction to fire propagation; it contributes hence to the convective cooling of the unburnt fuel and to pushing the flames into the vertical direction. Indeed, in the absence of slope and applied external wind, junction fire propagation is radiation dominated [14].

As shown in Figs. 6 and 7, the flow drawn from the lateral directions is globally perpendicular to the junction fire arms. For $\theta = 30°$, the combined actions of the flames tilt and the lateral flow (and resulting junction fire-arms distortion) before the deceleration phase (e.g., at $t - t_{Ign.} = 14$ s) results in a very fast fuel consumption around the junction point. Consequently, the angle between the junction fire arms increases and a trailing flaming "tail" is created (as shown at $t - t_{Ign.} = 24$ s) that does not contribute to the fire dynamics, and a new propagation phase (deceleration phase) starts with a lower ROS corresponding to a higher angle between the junction fire arms. This scenario does not occur for a junction angle $\theta = 60°$, because the flames are practically vertical and because the flow drawn from the lateral directions into the flaming zone does not push the fire arms towards the junction axis (see black arrows). In this case, induced flow drawn from the lateral directions acts uniformly on the junction fire arms during the entire propagation time, which explains the quasi-constant ROS obtained at high junction angles.

In order to examine the heat transfer modes governing junction fire spread, the rates of convective and radiative heat transfer received by the vegetation were investigated. The total density rate of heat transfer (convection + radiation) received by the solid fuel is given by Eq. (2), where T is the temperature of the gas mixture, T_s is the solid-fuel temperature, α_s and σ_s are respectively the fuel volume-fraction and surface-to-volume ratio, h_s is the convection heat transfer coefficient, σ is Stephan-Boltzmann constant, and J is the total irradiance. The convection heat transfer coefficient h_s is obtained from common empirical correlations relating the Nusselt and Reynolds numbers (based on the particle diameter) in the case of a flow across a long cylinder [18]. The total irradiance J is calculated by integrating the radiation intensity obtained by solving the radiative transfer equation in many directions [18].

$$\dot{g}_{tot} = \dot{g}_{conv} + \dot{g}_{rad} = h_s\alpha_s\sigma_s(T - T_s) + \frac{\alpha_s\sigma_s}{4}\left(J - 4\sigma T_s^4\right) \quad (2)$$

It should be noted that the density rate of heat transfer obtained from Eq. (2) are expressed in W/m^3 as they correspond to the rates absorbed by one cubic-meter of 'apparent' fuel volume (i.e., including the empty space of the volume occupied by the sparse fuel). A negative value of the heat transfer rate corresponds to a convective or a radiative cooling of the vegetation. As shown in Fig. 8, the contributions of convection and

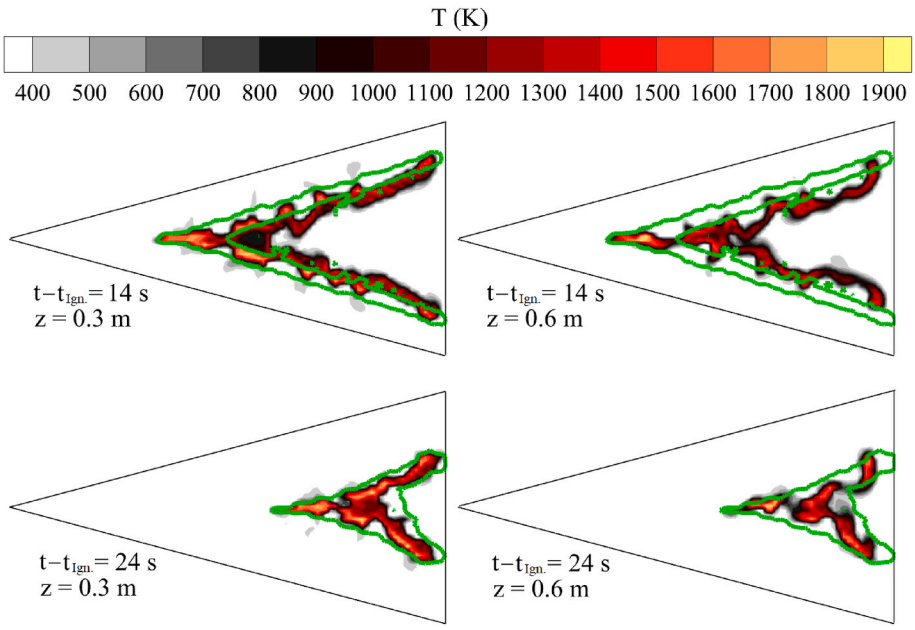

Fig. 4. Horizontal cuts (at $z = 0.3$ m and $z = 0.6$ m) of the temperature field obtained numerically 14 s and 24 s after ignition for a junction angle $\theta = 30°$, in the case of a horizontal terrain with no applied external wind. The black frame corresponds to the initial fuel-bed geometry. The green curve corresponds to the contour of the iso-value surface $T = 1000$ K at the vegetation top-surface (z = 0.15 m). (For interpretation of the references to colour in this figure legend, the reader is referred to the Web version of this article.)

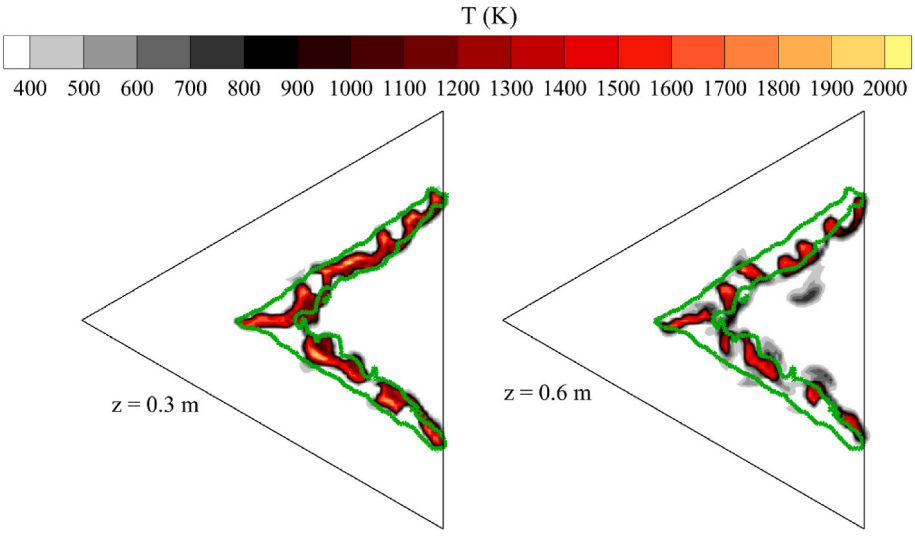

Fig. 5. Horizontal cuts (at $z = 0.3$ m and $z = 0.6$ m) of the temperature field obtained numerically 28 s after ignition for a junction angle $\theta = 60°$, in the case of a horizontal terrain with no applied external wind. The visuals definitions are the same as those in Fig. 4.

radiation to the total heat transfer to the unburnt fuel differ significantly. Both at $t - t_{Ign.} = 14$ s and 24 s (i.e., both in the acceleration and the deceleration phases of fire spread), radiation heat transfer to unburnt fuel (located to the right of the solid black curve corresponding to the pyrolysis front) is positive, while a convective cooling of unburnt fuel (negative heat transfer rate) resulting from fire-induced wind (shown in Fig. 6) is clearly observed. Consequently, junction fire spread is driven in this case by radiation heat transfer, as pointed out by previous experimental and numerical studies [12,14]. However, the deceleration in junction fire spread observed in this case cannot be attributed to convective processes, as suggested by Raposo et al. [12]. The interaction between the flames and fire-induced wind, resulting in an increase in the junction angle, is the mechanism responsible for the deceleration in the junction fire spread.

3.2. Slope and wind effects on flames-flow interaction

The effects of terrain slope and wind speed on the junction point ROS and on the heat transfer modes at laboratory scale were previously reported [12,14,15]. In this section, flames-flow interaction aspects are addressed by the same approach used in the case of a horizontal terrain with no applied external wind. As shown by Fig. 9, the junction point ROS increases both with the terrain slope and the prescribed wind speed. As previously reported [12,14,15], the deceleration phase at the end of fire spread is less pronounced on a sloping terrain or with imposed wind speed and does not occur in most instances. We notice local fire jumps resulting from local ignitions ahead of the junction point that specially occur when the flames reach the end of the fuel bed.

Fig. 10 shows that in the case of a relatively steep slope ($\alpha = 20°$), the

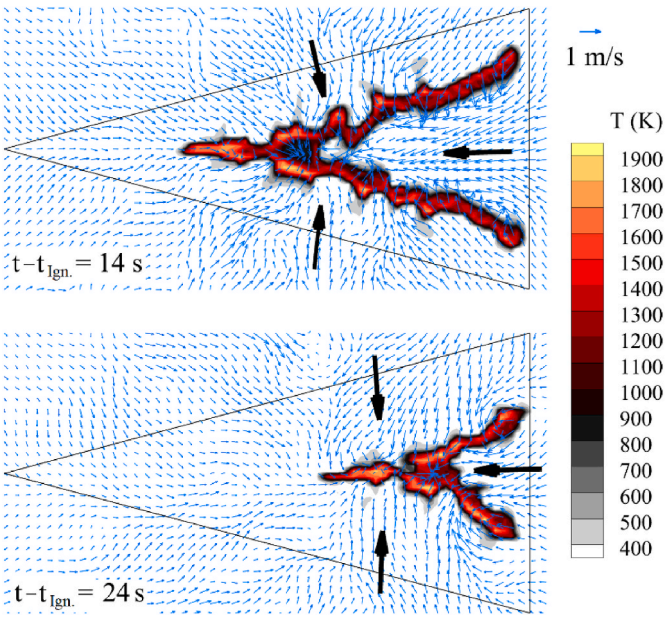

Fig. 6. Horizontal cuts at $z = 0.3$ m of the temperature field and corresponding flow velocity-vectors obtained numerically 14 s and 24 s after ignition for a junction angle $\theta = 30°$, in the case of a horizontal terrain with no applied external wind. The black frame corresponds to the initial fuel-bed geometry. The black arrows indicate the global flow action on the flames.

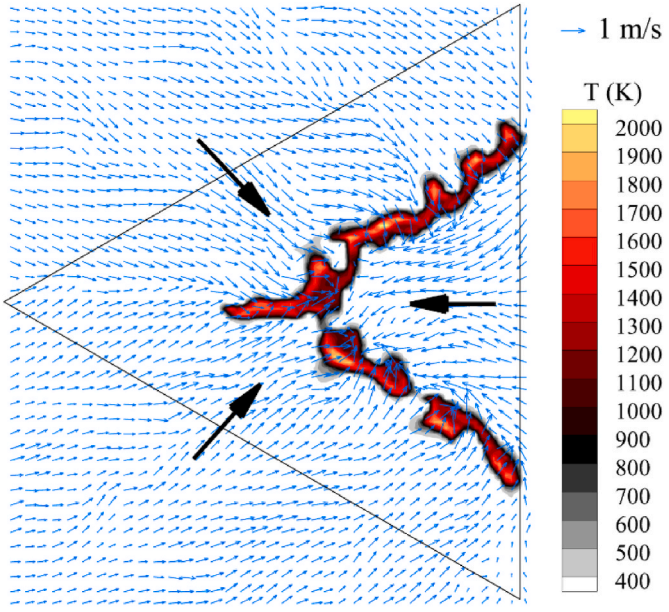

Fig. 7. Horizontal cut at $z = 0.3$ m of the temperature field and corresponding flow velocity-vectors obtained numerically 28 s after ignition for a junction angle $\theta = 60°$, in the case of a horizontal terrain with no applied external wind. The visuals definitions are the same as those in Fig. 6.

flames are totally tilted forward towards the unburnt fuel as shown by the horizontal cuts of the temperature field at $z = 0.3$ m and 0.6 m. This observation is consistent for the entire simulation time and for all considered cases carried out on a sloped terrain ($\alpha = 20°$ and 30°). In this case, the junction angle remained unchanged during the entire simulation time [14]. Consequently, a quasi-constant ROS of the junction point is obtained until the entire fuel volume was depleted. This behaviour was observed at small and large junction angles.

Fig. 11 shows that, in the case of relatively steep terrain, airflow is drawn from the lateral boundaries towards the V-shaped flaming region, which pushes the flames in the fire propagation direction. Compared to Fig. 6, although the junction angle is the same, flow direction onto and through the unburnt fuel has completely changed in Fig. 11. This has two important consequences for junction fire behaviour: 1 – this flow configuration prevents the increase of the angle between the junction fire arms and, consequently, the deceleration phase of the junction point propagation does not occur; 2 – flow direction results in convective heating of the unburnt fuel, in addition to radiative heat transfer. As the slope angle increases, convective heating of the unburnt fuel increases, and a transition from a radiation-dominated fire spread to a convective-dominated one occurs.

For a junction angle of 30°, Figs. 12 and 13 illustrate the effect of wind speed on flames structure for $U_0 = 1$ m/s. The flames in Fig. 12 are clearly tilted by the imposed wind towards the unburnt fuel, but the dominant characteristic in this case is the high irregularity in the flames' patterns, compared to Fig. 4. This evidently results from interaction with the flow field and is responsible for the perturbation in the junction point propagation shown in Fig. 12. Despite the imposed wind speed, Fig. 13 shows an important effect of induced wind on fire dynamics. We observe the formation of a trailing flaming tail (as in Fig. 6) that, however, remains in this case attached to the flaming zone by the action of the imposed wind, limiting any further widening of the angle between the junction fire arms. As a result, no deceleration phase is observed in fire spread, instead a jumping behaviour of the flame is obtained causing locally very high ROS values.

A clearer understanding of fire-induced wind can be obtained in this case by subtracting from the flow field obtained at $z = 0.3$ m, $u(x,y)$, the prevailing wind speed $U_{0.3}$ obtained from Eq. (1) at $z = 0.3$ m and equal to 0.842 m/s for $U_0 = 1$ m/s. Fig. 13-bottom shows that the resulting flow field, $u(x,y) - U_{0.3}$, appears to be nearly perpendicular to the junction fire arms. It should be noted in this case that, according to Fig. 13, the characteristic velocity of the induced-wind field is comparable to imposed wind speed. This competition between imposed wind and induced wind may explain the high irregular character observed in the flames' patterns. It is worth noting that it is practically impossible to entirely isolate induced wind from the flow field, and Fig. 13-bottom does not accurately show fire-induced flow. In particular, the method overestimates the intensity of induced wind in the regions where the effect of imposed wind is reduced (such as between the junction arms). However, since a qualitative analysis of the action of induced wind is carried out rather than a quantitative one, the conclusions drawn from Fig. 13-bottom remain true. As shown by Fig. 14, similar fire dynamics are obtained for other junction angles at low wind speeds as a result of the competition between the imposed and fire-induced winds. As the imposed wind speed increases and becomes the dominant component of the flow field, regular fire dynamics is again observed, as shown by Fig. 15 for $U_0 = 3$ m/s. Hence, for the considered fuel properties and junction size, a wind speed $U_0 = 1$ m/s seems to result in a transitional regime preceding a wind-driven regime of fire propagation.

4. Conclusion

This study provides some insights into the dynamics of junction fires at laboratory scale, focusing on the action of induced wind and on the mechanisms responsible for the deceleration in fire spread observed under certain conditions. Full-physical modelling of junction fires was conducted using FIRESTAR3D and an analysis of fire behaviour was carried out based on the interaction between the flames' structure and the surrounding flow field. In the case of a junction fire on a horizontal terrain with no imposed wind, results show that the deceleration in fire spread, observed both experimentally and numerically for small junction angles, is caused by a change in flame inclination and the trailing flame separation resulting in a widening of the angle between the junction fire arms, and consequently in a lower ROS. For a large junction angle, flames remain vertical due to the low interaction between the

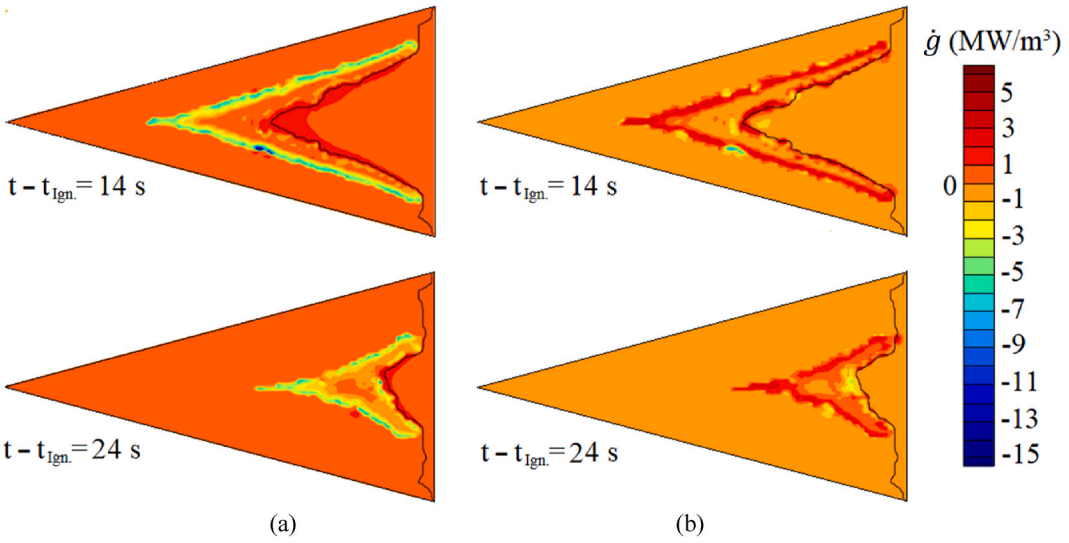

Fig. 8. Distribution of the radiative (a) and convective (b) density rates of heat transfer received at the vegetation top-surface ($z = 0.15$ m), obtained 14 s and 24 s after ignition, for a junction angle $\theta = 30°$, in the case of a horizontal terrain with no applied external wind. The black curve corresponds to the pyrolysis-front position at the vegetation surface.

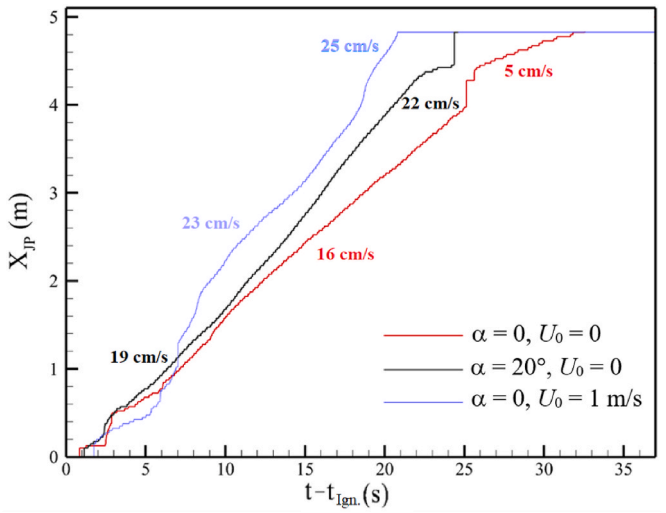

Fig. 9. Time evolution of the junction point position obtained for a junction angle $\theta = 30°$ and for three combinations of terrain slope and wind speed: ($\alpha = 0$, $U_0 = 0$), ($\alpha = 20°$, $U_0 = 0$) and ($\alpha = 0$, $U_0 = 1$ m/s). Average ROS values are indicated at different phases of fire propagation.

junction fire arms and induced-flow uniformly pushes the junction arms during the entire propagation time, which does not allow for the scenario that takes place for a small junction angle to occur, and a quasi-constant ROS is recorded during the entire fire-propagation time. Terrain slope and external wind have significant effects on the fire dynamics. A junction fire on sloping terrain did not exhibit a deceleration phase (at least for the considered slopes), as induced-wind direction, aligned with the direction of fire spread, results in stable fire propagation with no change in the angle between the junction fire arms. Similarly, imposing a relatively large wind speed increased the flame tilt towards unburnt fuel, resulting in a stable, wind-driven fire propagation. However, at a relatively low wind speed, the competition between the imposed wind and the fire-induced wind results in erratic fire dynamics and spread. The study offers new insights into the development of fire-induced wind and its interaction with the flaming zone. Results showed that the induced wind is globally normal to the junction fire arms. This simple observation is important for developing scaling laws for junction fires, similar to those developed for a straight fire line, where the actions of cross-wind, slope, buoyancy, and induced wind on the fire front are considered [23]. The study also highlighted the importance of fully-physical modelling in wildfire research, particularly in unravelling the reasons behind observed global behaviours. Future work can build on this by establishing extrapolation frameworks that translate small-scale findings to large-scale or real-world conditions, guided by scaling laws based on relevant dimensionless numbers. This

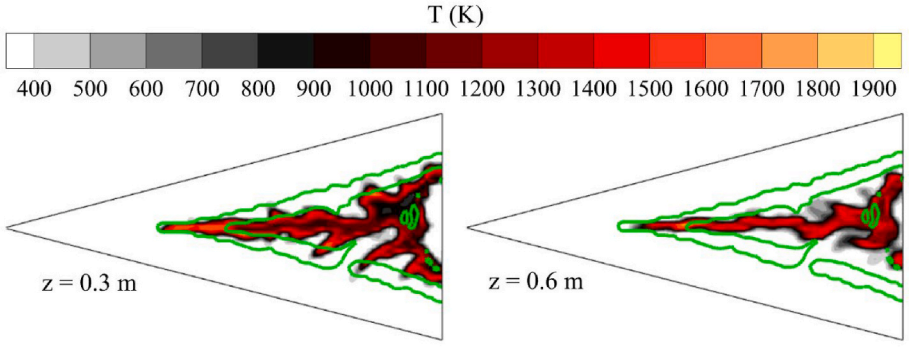

Fig. 10. Horizontal cuts (at $z = 0.3$ m and $z = 0.6$ m) of the temperature field obtained numerically 14 s after ignition for a junction angle $\theta = 30°$, a terrain slope $\alpha = 20°$, and no imposed wind. The visuals definitions are the same as those in Fig. 4.

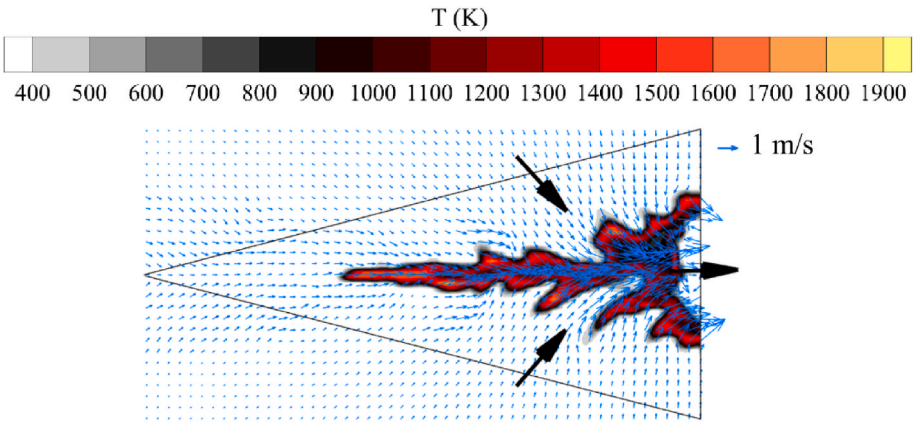

Fig. 11. Horizontal cut at $z = 0.3$ m of the temperature field and corresponding flow velocity-vectors obtained numerically 14 s after ignition for a junction angle $\theta = 30°$, a terrain slope $\alpha = 20°$, and no imposed wind. The visuals definitions are the same as those in Fig. 6.

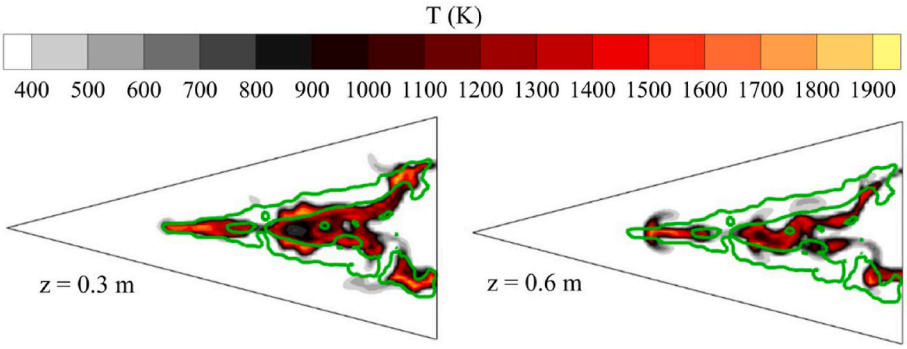

Fig. 12. Horizontal cuts (at $z = 0.3$ m and $z = 0.6$ m) of the temperature field obtained numerically 14 s after ignition for a junction angle $\theta = 30°$, on a horizontal terrain and imposed wind speed $U_0 = 1$ m/s. The visuals definitions are the same as those in Fig. 4.

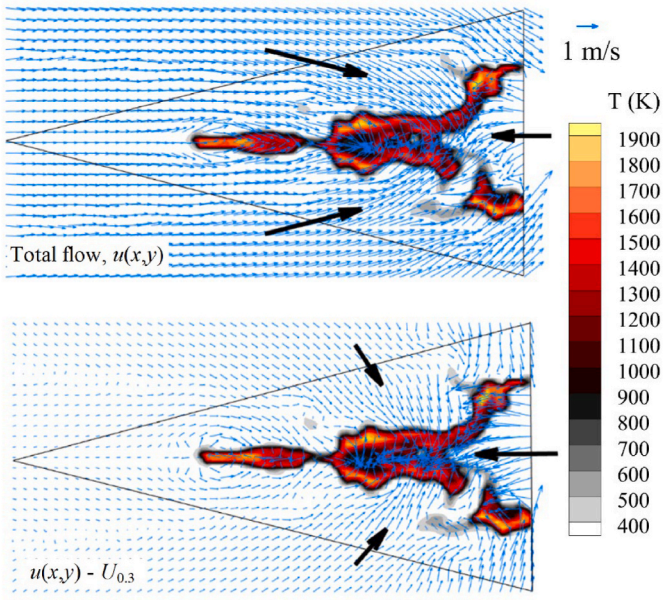

Fig. 13. Horizontal cut at $z = 0.3$ m of the temperature field and corresponding flow velocity-vectors obtained numerically 14 s after ignition for a junction angle $\theta = 30°$, on a horizontal terrain and imposed wind speed $U_0 = 1$ m/s. Top: total flow field $u(x,y)$. Bottom: $u(x,y) - U_{0.3}$, where $U_{0.3}$ is obtained Eq. (1) at $z = 0.3$ m. The visuals definitions are the same as those in Fig. 6.

would also enable the quantification of the so-called "junction effect" (the observed surplus in ROS that occurs when two fire fronts merge), hence improve both theoretical understanding and predictive capability across scales.

CRediT authorship contribution statement

Ahmad Hassan: Writing – original draft, Visualization, Validation, Software, Resources, Project administration, Methodology, Investigation, Formal analysis, Data curation, Conceptualization. **Gilbert Accary:** Writing – review & editing, Supervision, Software, Project administration, Conceptualization. **Jason Sharples:** Writing – review & editing, Supervision, Project administration, Conceptualization. **Khalid Moinuddin:** Writing – review & editing, Supervision, Project administration, Conceptualization.

Novelty and significance statement

This study introduces a novel understanding of the dynamics of small-scale junction fires through advanced physical modelling techniques. By leveraging high-fidelity simulations using a fully physical modelling approach, the research provides new insights into the mechanisms responsible for the deceleration of the junction point propagation and into the flow characteristics of merging fire lines. The assessment of flame and flow properties through a fully physical model offers a distinctive methodology that relies solely on scientific explanations, avoiding assumptions. This approach elucidates behaviours observed in junction fires, such as rapid spread and subsequent deceleration, while also enabling evaluation of key junction fire properties under varying wind and slope conditions. This work addresses a critical

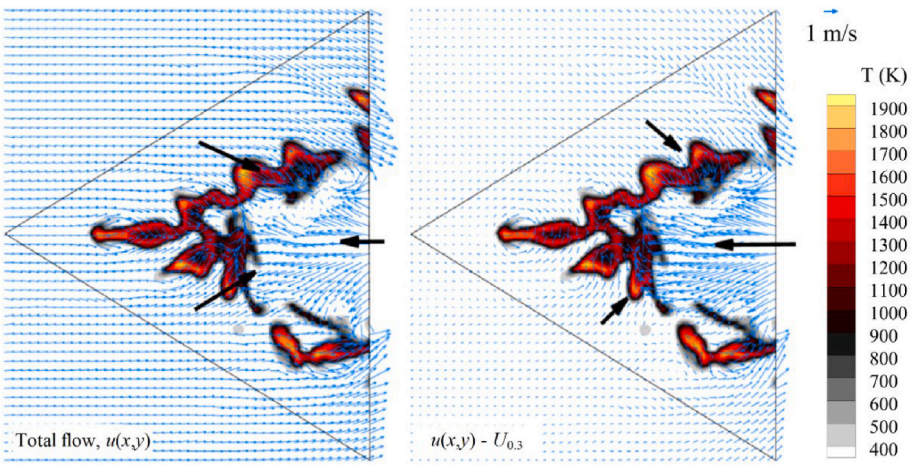

Fig. 14. Horizontal cut at $z = 0.3$ m of the temperature field and corresponding flow velocity-vectors obtained numerically 14 s after ignition for a junction angle $\theta = 60^{\circ}$, on a horizontal terrain and imposed wind speed $U_0 = 1$ m/s. Left: total flow field $u(x,y)$. Right: $u(x,y) - U_{0.3}$, where $U_{0.3}$ is obtained Eq. (1) at $z = 0.3$ m. The visuals definitions are the same as those in Fig. 6.

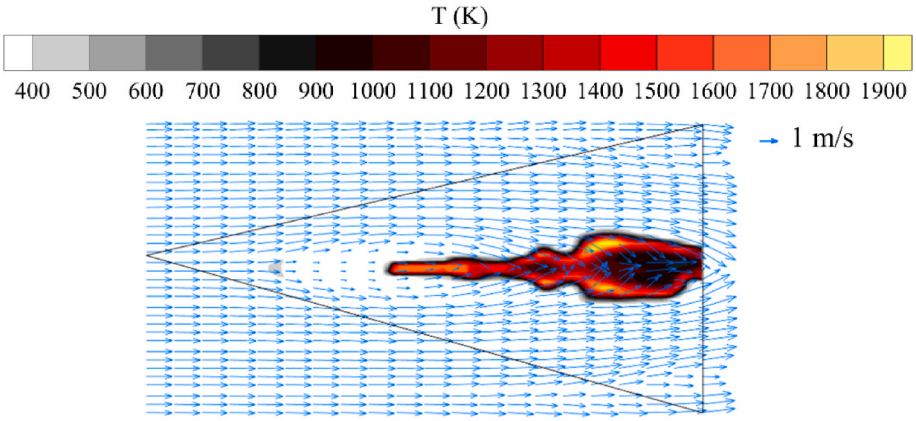

Fig. 15. Horizontal cut at $z = 0.3$ m of the temperature field and corresponding flow velocity-vectors obtained numerically 14 s after ignition for a junction angle $\theta = 30^{\circ}$, on a horizontal terrain and imposed wind speed $U_0 = 3$ m/s. The black frame corresponds to the initial fuel-bed geometry.

gap in wildfire research by clarifying complex interaction patterns and lays the groundwork for future advancements in fire modelling and understanding of extreme wildfire phenomena.

Declaration of competing interest

The authors declare the following financial interests/personal relationships which may be considered as potential competing interests: Ahmad Hassan reports financial support was provided by Natural Hazards Research Australia. If there are other authors, they declare that they have no known competing financial interests or personal relationships that could have appeared to influence the work reported in this paper. No personal relationship with Natural Hazards Research Australia. Natural Hazards Research Australia provide partial funds for my PhD project in Victoria University.

Acknowledgments

Aix-Marseille University computing-centre is acknowledged for granting access to its HPC resources. This work is partially funded by Natural Hazards Research Australia and Victoria University.

Appendix A. FIRESTAR3D Model

FIRESTAR3D is a fully physical, CFD model, based on a multiphase formulation [18,20]. The model predicts the behaviour of the coupled system consisting of a turbulent-reactive gaseous flow (fluid phase) interacting with a vegetative fuel (solid phase) represented as a porous medium. The evolution of each phase is governed by a set of conservation equations (solved using two independent grids) with source/sink terms representing the interaction between the two phases.

The mathematical model of the fluid phase consists of the conservation equations of mass, momentum, energy and chemical species resulting from vegetation decomposition. The model is solved using the standard finite volume method on a structured mesh; the method is third-order accurate in space and time. The radiation transfer equation is solved using the Discrete Ordinate Method (DOM) or S_N approximation, which consists in the calculating the radiation intensity in $N \times (N + 2)$ finite number of directions; then, the total irradiance is calculated by integrating the radiative intensity in all directions, i.e., over 4π steradians [20]. The reported simulations were performed using S_8 approximation with a total number of 80

discrete directions. The code employs a large-eddy simulation (LES) turbulence-model and radiation-turbulence-interaction model [20]. The combustion in the gaseous phase is based on CO kinetics using an Eddy Dissipation Concept model to evaluate the combustion rate occurring in the gaseous phase [18].

The degradation of the vegetation in FIRESTAR3D model is governed by three temperature-dependent mechanisms: drying, pyrolysis, and charcoal combustion. The fourth-order Runge-Kutta method is used to solve (on an independent grid) the solid-phase model describing the decomposition of the vegetation as a result of the intense heat flux coming from the flaming zone [18]. The constants of the model associated with the charcoal combustion (activation energy and pre-exponential factor) are evaluated empirically from a thermal analysis conducted on various solid fuels samples. Thermogravimetry analysis (TGA) shows that for temperatures about 1000 K, the gas mixture produced by pyrolysis during the decomposition of forest fuel was primarily composed of CO, CO_2, followed by CH_4 and in less proportion of H_2, C_2H_6 [24]. Then, hydrocarbon compounds quickly react with O_2 in ambient air resulting in CO, CO_2 and H_2O. However, in FIRESTAR3D, a simplified representation is considered with one-step reaction (assuming hydrocarbon compounds combustion to be complete and quasi-instantaneous) resulting in a gas mixture that only includes the primarily and final gaseous species, CO and CO_2, along with O_2, H_2O, and N_2 [25]. Hence, the combustion in the gaseous phase is based on CO kinetics.

Appendix B. Model Validation

This section presents a summary of a previously reported validation work of junction fire modelling using FIRESTAR3D, in addition to a mesh-sensitivity analysis carried out for the main cases reported in this study.

Junction fire modelling using FIRESTAR3D has been validated against experimental tests [2] conducted at the Forest Fire Research Laboratory (LEIF). While the primary criterion for assessing the model was the ROS, qualitative features were also considered. Experimental junction fires were reproduced numerically and environmental conditions such as temperature, humidity, and fuel properties (e.g., moisture content and heat capacity) were accounted for, along with the fuel-layer geometry and ignition process [13]. The fuel (shrubs) was modelled using two approaches: a single representative element with average properties and a two-element model distinguishing between leaves and twigs. The single-element approach was found to be more effective and representative.

As shown by Fig. B1, a uniform mesh was used for the solid phase, while for the fluid one, a uniform mesh was used in the solid-phase region, then the fluid-phase mesh was progressively coarsened towards the open boundaries of the computational domain. For the mesh-sensitivity analysis, the three meshes reported in Tab. B1 were considered. The results reported in this work were obtained using the "Study mesh". The simulations were performed using the adaptative time-stepping strategy, with a time step between 10^{-2} and 10^{-3} s. At each time step, the solution was assumed obtained when the L_2-norm of all transport equations residuals reached 10^{-5} (in normalized form) or 10^{-4} (in non-normalized form). The simulations were performed on a 16-cores node. One second of real simulation time required around 80 h of CPU time (i.e., about 5 h of elapsed real time per second of real simulation time).

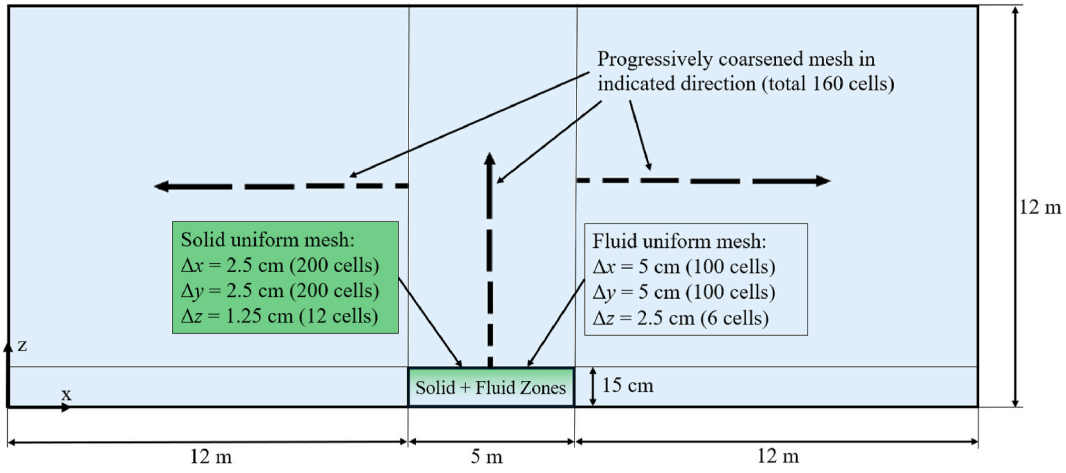

Fig. B1. Mesh in the vertical median plane used for a junction angle $\theta = 30°$. Light blue (fluid domain), green (solid domain). Fuel region dimension is stretched in z-direction for more clarity. In y-direction, mesh is uniform in the fuel region, then progressively coarsened toward the open boundaries with a total of 160 cells.

Tab. B1
Grid size used in the mesh-sensitivity analysis (case of for a junction angle $\theta = 30°$). The results reported in this work were obtained using the "Study mesh".

Mesh main parameters	Finer mesh	Study mesh	Coarser mesh
Minimum cells size in the (x,y) plane	3.125 cm	5 cm	7 cm
Fluid-phase domain mesh-size	240 × 160 × 200	160 × 112 × 160	112 × 78 × 120
Solid-phase domain mesh-size	321 × 161 × 17	201 × 105 × 13	145 × 77 × 11

As shown by Fig. B2, the mesh size has little effect on the ROS (the average slopes of the curves) and on the existence of the deceleration phase observed at small junction angles. The differences obtained between the various considered meshes result mainly from the ignition phase since the burner's width (hence intensity) depends on the mesh size (grid resolution) in the x-y plane, as well as from the fact that the junction point position shown in the figure is tracked at a single point in the fuel bed.

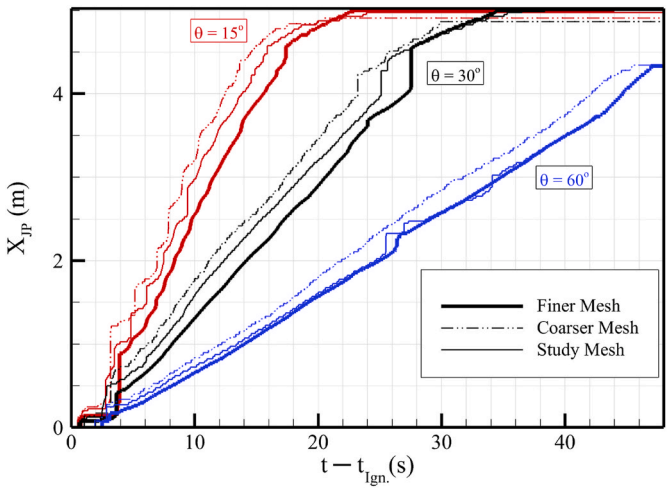

Fig. B2. Time evolution of the junction point position of the three cases sown in Fig. 3 (three junction angles, horizontal terrain, no applied external wind) obtained for the three meshes reported in Tab. B1.

Appendix C. Previously-Reported Junction Fire Results

Previously-reported results showed that the FIRESTAR3D model successfully captures key junction fire characteristics, enabling detailed simulations across a wide range of parameters, including conditions that are difficult to study experimentally. A summary of the effects of terrain slope, junction angle, and wind speed on junction fire global behaviour is presented in this section. A detailed discussion of these effects can be found in the published parametric studies [14,15].

As expected in a typical fire behaviour, an increase in slope angle and/or wind speed generally leads to an increase in the junction point ROS. However, this trend is influenced by the junction angle. Generally, an increase in junction angle results in a reduction in the ROS as shown in Fig. C1. This can be explained by a change in the interaction nature between the two merging firearms. Nevertheless, even at wider junction angles, such as 90°, junction effect is still important and the ROS is significantly lager compared to a single line propagation. As shown in Fig. C1, narrow junction angles (15° and 30°) are associated with a deceleration phase during the final stage of propagation on a horizontal terrain. Interestingly, this deceleration does not occur when the fire propagates on a slope, indicating that slope plays a crucial role in sustaining higher spread rates during junction formation.

Fig. C2 shows the rate of radiation heat transfer received by the entire vegetation layer. A positive heat rate indicates that the fuel receives more energy than it emits. No clear correlation was found between the acceleration/deceleration of the junction fire (observed for instance for $\alpha = 0°$ and $\theta = 30°$) and the radiative (or convective) heat transfer rate. Instead, the results suggest typical behaviour: as wind speed or terrain slope angle increases, the contribution of radiation to the overall heat transfer rate to the vegetation decreases, and convection becomes the dominant mode of heat transfer.

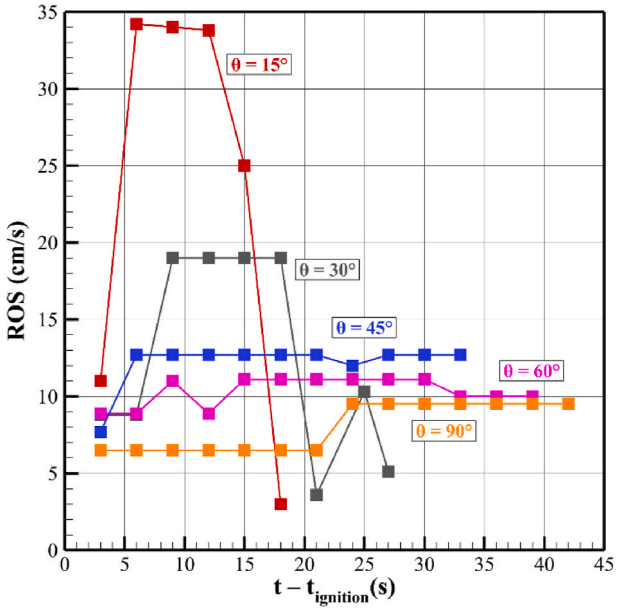

Fig. C1. Time evolution of the junction point ROS on a horizontal terrain ($\alpha = 0°$) for different junction angles.

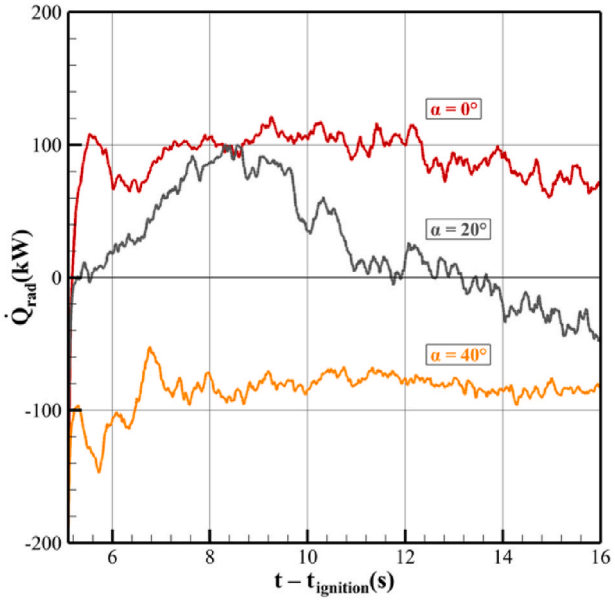

Fig. C2. Time evolution of the rates of radiation heat transfer received by the entire fuel volume for a junction angle of 30° and different terrain slope angles.

Data availability

Data will be made available on request.

References

[1] D.X. Viegas, C. Ribeiro, M. Almeida, P. Pinto, L.M. Ribeiro, Á. Silva, Field and laboratory analysis of the junction fire process in the catastrophic fire of Pedrógão Grande in June 2017, Int. J. Wildland Fire 32 (6) (2023) 951–967, https://doi.org/10.1071/WF22161.

[2] D.X. Viegas, J.R. Raposo, D.A. Davim, C.G. Rossa, Study of the jump fire produced by the interaction of two oblique fire fronts. Part 1. Analytical model and validation with no-slope laboratory experiments, Int. J. Wildland Fire 21 (7) (2012) 843–856, https://doi.org/10.1071/WF10155.

[3] C. Np, Origin and Development of the Bushfires that Spread into the ACT, 8–18 January 2003, 2005.

[4] D. Viegas, J. Raposo, A. Figueiredo, Preliminary analysis of slope and fuel bed effect on jump behavior in forest fires, Procedia Eng. 62 (2013) 1032–1039, https://doi.org/10.1016/j.proeng.2013.08.158.

[5] J. Sharples, I. Towers, G. Wheeler, V. Wheeler, J. McCoy, Modelling fire line merging using plane curvature flow, in: J. Piantadosi, R.S. Anderssen, J. Boland (Eds.), *20th International Congress on Modelling and Simulation*, Adelaide, South Australia, 2013. https://ro.uow.edu.au/eispapers/1792/.

[6] C.M. Thomas, J.J. Sharples, J.P. Evans, Modelling the dynamic behaviour of junction fires with a coupled atmosphere–fire model, Int. J. Wildland Fire 26 (4) (2017) 331–344, https://doi.org/10.1071/WF16079.

[7] J.E. Hilton, A.L. Sullivan, W. Swedosh, J. Sharples, C. Thomas, Incorporating convective feedback in wildfire simulations using pyrogenic potential, Environ. Model. Software 107 (2018) 12–24, https://doi.org/10.1016/j.envsoft.2018.05.009.

[8] A.L. Sullivan, W. Swedosh, R.J. Hurley, J.J. Sharples, J.E. Hilton, Investigation of the effects of interactions of intersecting oblique fire lines with and without wind in a combustion wind tunnel, Int. J. Wildland Fire 28 (9) (2019) 704–719, https://doi.org/10.1071/WF18217.

[9] L. Merino, F. Caballero, J.R. Martínez-de-Dios, I. Maza, A. Ollero, An unmanned aircraft system for automatic forest fire monitoring and measurement, J. Intell. Rob. Syst. 65 (1) (2012) 533–548, https://doi.org/10.1007/s10846-011-9560-x.

[10] A. Filkov, B. Cirulis, T. Penman, Quantifying merging fire behaviour phenomena using unmanned aerial vehicle technology, Int. J. Wildland Fire 30 (3) (2021) 197–214, https://doi.org/10.1071/WF20088.

[11] B. Holyland, B. Cirulis, T.D. Penman, A.I. Filkov, The effects of junction fire development on thermal behaviour at the field scale, Fire Saf. J. 143 (2024) 104057, https://doi.org/10.1016/j.firesaf.2023.104057.

[12] J.R. Raposo, et al., Analysis of the physical processes associated with junction fires at laboratory and field scales, Int. J. Wildland Fire 27 (1) (2018) 52–68, https://doi.org/10.1071/WF16173.

[13] A. Hassan, G. Accary, D. Sutherland, S. Méradji, K. Moinuddin, Physics-based modelling of junction fires: sensitivity and validation studies, in: D.X.V.L. M. Ribeiro (Ed.), IX International Conference on Forest Fire Research, 2022, pp. 315–322, https://doi.org/10.14195/978-989-26-2298-9_50.

[14] A. Hassan, G. Accary, D. Sutherland, K. Moinuddin, Physics-based modelling of junction fires: parametric study, Int. J. Wildland Fire 32 (3) (2023) 336–350, https://doi.org/10.1071/WF22121.

[15] A. Hassan, G. Accary, D. Sutherland, K. Moinuddin, Physics-based modelling of wind-driven junction fires, Fire Saf. J. 142 (2024) 104039, https://doi.org/10.1016/j.firesaf.2023.104039.

[16] N. Frangieh, G. Accary, D. Morvan, S. Méradji, O. Bessonov, Wildfires front dynamics: 3D structures and intensity at small and large scales, Combust. Flame 211 (2020) 54–67, https://doi.org/10.1016/j.combustflame.2019.09.017.

[17] K. Moinuddin, M. Kyng, A. Hassan, G. Accary, Physical modelling of dynamic bushfire propagation leading to parameterization for operational modelling, in: T. Z. Hassan MK, M.D. Hossain, S. Pathirana, A. Todhunter (Eds.), The International Conference on Fire Safety Engineering Research and Practice, Icfserp 2024 Conference, 2024, p. 734. Sydney, Australia.

[18] D. Morvan, G. Accary, S. Meradji, N. Frangieh, O. Bessonov, A 3D physical model to study the behavior of vegetation fires at laboratory scale, Fire Saf. J. 101 (2018) 39–52, https://doi.org/10.1016/j.firesaf.2018.08.011.

[19] K. Moinuddin, C. Tirado Cortes, A. Hassan, G. Accary, F. Wu, Simulation of rare fire event scenarios using fully-physical models and visualisation systems, in: D. Del Favero, S. Thurow, M.J. Ostwald, U. Frohne (Eds.), Climate Disaster Preparedness, 1 ed., Springer Cham, 2024, p. 219, ch. Chapter 1.4.

[20] G. Accary, D. Morvan, How can CFD contribute to the understanding of wildfire behaviour? Comput. Fluid 279 (2024) 106322 https://doi.org/10.1016/j.compfluid.2024.106322.

[21] D. Morvan, Physical phenomena and length scales governing the behaviour of wildfires: a case for physical modelling, Fire Technol. 47 (2) (2011) 437–460, https://doi.org/10.1007/s10694-010-0160-2.

[22] J. Fayad, et al., Numerical study of an experimental high-intensity prescribed fire across Corsican Genista salzmannii vegetation, Fire Saf. J. 131 (2022) 103600, https://doi.org/10.1016/j.firesaf.2022.103600 (in English).

[23] D. Morvan, G. Accary, How to Properly Account for Slope Effect in Byram's Convective Number? A New Proposal, Fire Technology, 2024.

[24] A.M. Grishin, F. Albini (Eds.), Mathematical Modeling Forest Fire and New Methods Fighting Them, Publishing House of the Tomsk State University, 1997, p. 390.

[25] D. Morvan, J.L. Dupuy, Modeling of Fire Spread Through a Forest Fuel Bed Using a Multiphase Formulation, 127, Combustion & Flame, 2001, pp. 1981–1994.